

Relativistic Ritz approach to hydrogen-like atoms II: spectral analysis of hydrogen and deuterium

David M. Jacobs*

*Physics Department, Norwich University, 158 Harmon Dr, Northfield, VT 05663, USA and
CERCA, Physics Department, Case Western Reserve University, Cleveland, OH 44106, USA*

(Dated: November 14, 2022)

A long-distance effective theory of hydrogen-like atoms, dubbed the relativistic Ritz approach was recently introduced and some its theoretical consequences were explored. In this article, the relativistic Ritz approach is used to fit extant measurements of atomic hydrogen and deuterium transitions using information-theoretic analyses. As a result, the fine-structure constant (α), a fundamental parameter of the Standard Model, may be determined simultaneously with the ionization energies of hydrogen and deuterium, $E_I^{(H)}$ and $E_I^{(D)}$. The best hydrogen analysis yields $\alpha^{-1} = 137.035\,999\,185(25)$, in good agreement with the value obtained by other methods and without relying on a separately determined Rydberg constant. From the same analysis, I find that $E_I^{(H)} = 13.598\,434\,599\,684(25)$ eV, an improvement of two orders of magnitude in precision compared to previous determinations and in agreement with the Standard Model prediction at 1.8 parts per trillion. The best deuterium analysis yields $E_I^{(D)} = 13.602\,134\,636\,543(31)$ eV, agreeing with the Standard Model at 2.3 parts per trillion. This study demonstrates how the relativistic Ritz approach can be used for testing the Standard Model with the spectra of hydrogen-like atoms.

I. INTRODUCTION

The Standard Model of particle physics describes the fundamental interactions between particles on the smallest length scales. Despite its many successes, there are several apparent problems with the model. For example, it does not account for the observation of neutrino oscillations nor does it provide an explanation for the excess of matter over antimatter in the Universe [1, 2]. Where gravity is concerned, there are other mysteries; for example, the mass in the Universe in the form of Standard Model particles was incapable of gravitationally coalescing on its own to form the astrophysical structure observed today [3]. Testing the Standard Model at high precision thus remains a primary motivation to perform new physics experiments. High-energy particle colliders have, historically, provided a wealth of information about fundamental particle physics, but as the energies of these colliders has increased so has their cost, making the construction of new colliders harder to justify.

In recent decades it has become apparent that high-precision experiments involving atoms and molecules are a complementary means to test the Standard Model and to probe for new physics [4]. Such experiments include measurements of the transitions between atomic states and are accompanied by either the emission or absorption of photons whose energy can be precisely measured. The most precise experiments are performed with *hydrogen-like* systems, which include deuterium and positronium¹.

Additionally, atomic measurements allow for the determination of some of the fundamental constants of the Standard Model. In particular, the fine-structure constant

$$\alpha = \frac{e^2}{4\pi\epsilon_0\hbar c}, \quad (1)$$

quantifies the strength of the electromagnetic interaction and plays a pivotal role in physics and chemistry. Independent methods of measuring such constants are crucial both for building confidence in those values and also for testing the theory.

Bound-state quantum electrodynamics (BSQED) is the primary theoretical tool within the Standard Model for predicting the energy levels of atoms and for extracting fundamental constants from atomic spectra. Improving the precision of the theory is challenging (see, e.g., [6]), while spectroscopy may be subject to unanticipated sources of error [7]. Recently, a semi-empirical theory for hydrogen-like atoms has been developed, dubbed the *relativistic Ritz* approach [8, 9]. The approach rests on the fact that atomic effects beyond the lowest-order Coulomb interaction can be categorized by one of two types: (1) kinetic relativistic effects ($v/c > 0$) and (2) shorter-ranged interactions, such as those associated with spin coupling, vacuum polarization, particle self-energy, and finite particle size.

Within the Standard Model, the largest length scale associated with these effects is the (reduced) Compton wavelength of the electron, $r_{\text{QED}} = \hbar/(m_e c)$, whereas the orbital scale of the hydrogen atom in the n 'th level is $r_{\text{atom}} = r_{\text{QED}} n^2 / \alpha \simeq 137 r_{\text{QED}} n^2$. By analyzing the quantum dynamics at long distance, i.e., $r_{\text{atom}} \gg r_{\text{QED}}$, it is possible to treat both the electron and nucleus as relativistic point-like objects and “work inward”, account-

* djacobs@norwich.edu

¹ See, e.g., [5] for recent developments on measurements of this system, composed of an electron bound with a positron.

ing for the omitted short-ranged interactions empirically through a low-energy series expansion of the quantum defect, δ . For hydrogen and deuterium, this long-distance criterion is true even for the ground state. The relativistic Ritz approach supersedes the older non-relativistic Ritz approach as a means to interpolate between and extrapolate beyond measured transitions[8]; however, in this article it will be shown that the method may also be used to extract quantities relevant to the Standard Model, namely the atomic ionization energy, E_I , and the fine-structure constant, α .

Given what will be demonstrated here, i.e., what the relativistic Ritz approach can accomplish with regard to spectroscopic data, it is useful to take stock of the methods that have been used hitherto to obtain ionization energies empirically, what the Standard Model predictions of those ionization energies are, as well as how some determinations of α are made.

To begin with, the canonical (nonrelativistic) Rydberg-Ritz fitting formula has historically been used to fit spectral data of alkali atoms, as well as atomic hydrogen and deuterium. This formula is

$$E_I - E_n = \frac{hcR_\infty Z^2}{1 + \frac{m_e}{M_N}} \frac{1}{(n - \delta)^2}, \quad (2)$$

where E_n are the term energies, $hcR_\infty = m_e c^2 \alpha^2 / 2$ is the Rydberg-Hartree energy, Z and M_N are the nuclear charge and mass, respectively. Throughout this article, the defined CODATA [10] values $h = 6.626\,070\,15 \times 10^{-34}$ J·s, $c = 299\,792\,458$ m/s, and $e = 1.602\,176\,634 \times 10^{-19}$ C are used. The following (even-only) modified Ritz formula is often used as an ansatz for the quantum defect,

$$\delta = c_0 + \frac{c_2}{(n - c_0)^2} + \frac{c_4}{(n - c_0)^4} + \frac{c_6}{(n - c_0)^6} + \dots \quad (3)$$

In Ref. [11], this fitting formula was used to extract the atomic hydrogen ionization energy from spectral data contained within the ASD [12],

$$\begin{aligned} E_I^{(\text{H,data})} &= 3\,288\,086\,856.8(7) \text{ MHz} \times h \\ &= 13.598\,434\,598(3) \text{ eV}. \end{aligned} \quad (4)$$

which is in agreement with the Standard Model prediction[12],

$$E_I^{(\text{H,SM})} = 13.598\,434\,599\,702(12) \text{ eV}, \quad (5)$$

at the level of 2×10^{-10} . Likewise, the deuterium ionization energy is determined to be

$$\begin{aligned} E_I^{(\text{D,data})} &= 3\,288\,981\,521.1(2.3) \text{ MHz} \times h \\ &= 13.602\,134\,633(10) \text{ eV}. \end{aligned} \quad (6)$$

which agrees with the Standard Model prediction,

$$E_I^{(\text{D,SM})} = 13.602\,134\,636\,569(12) \text{ eV}, \quad (7)$$

at the level of 7×10^{-10} . As described in the sections that follow, I will improve upon the data-derived results of (4) and (6) by more than two orders of magnitude by using the relativistic generalization of equation (2).

As for the fine-structure constant, α , in recent years, its most precise determinations have come by one of two means: (1) from the comparison of the experimentally determined electron g-factor [13] with the theoretical prediction [14] and (2) atomic recoil experiments involving rubidium [15] or cesium [16], combined with a chain of relative mass measurements [17] and the Rydberg constant [10], R_∞ . The Rydberg constant is determined from certain measured hydrogen and deuterium transitions, analyzed using BSQED. Recent determinations of the inverse fine-structure constant, α^{-1} , are listed in Table I.

TABLE I. A selection of fine-structure constant determinations.

α^{-1}	Type	Reference
137.035 999 166(15)	electron g-factor/QED	[14, 18]
137.035 999 150(33)	electron g-factor/QED	[13, 14]
137.035 999 046(27)	atom recoil/BSQED	[16]
137.035 999 206(11)	atom recoil/BSQED	[19]

Here I apply the relativistic Ritz approach to extract atomic hydrogen and deuterium spectroscopic data, demonstrating a new method for testing bound-state QED and the Standard Model, as well as checking for internal consistency of spectroscopic data. The former is done through the simultaneous determination of the ground state ionization energies and α with a precision that is competitive with the references mentioned above. In Section II I will summarize the approach and its input parameters for use in spectral analysis. In Sections III and IV I analyze publicly available hydrogen and deuterium data, respectively. I conclude with a discussion in Section V.

II. PRELIMINARIES

A. Model summary, input parameters, and fitting procedure

The energy levels of a hydrogen-like atom composed of two particles of mass m_1 and m_2 were shown in the relativistic Ritz approach [8] to be

$$E_n = \sqrt{m_1^2 + m_2^2 + \frac{2m_1 m_2}{\sqrt{1 + \left(\frac{Z\alpha}{n_\star}\right)^2}}} - (m_1 + m_2), \quad (8)$$

where the effective quantum number,

$$n_\star = n - \delta. \quad (9)$$

The quantum defect, δ , causes an eigenfunction to deviate from its canonical “pure Coulomb” form and accounts for omitted short-ranged interactions [20–23]. One may

$$\delta = \delta_{(0)\ell j} + \frac{\delta_{(2)\ell j}}{(n - \delta_{(0)\ell j})^2} + \frac{\delta_{(4)\ell j}}{(n - \delta_{(0)\ell j})^4} + \frac{2\delta_{(2)\ell j}^2}{(n - \delta_{(0)\ell j})^5} + \frac{\delta_{(6)\ell j}}{(n - \delta_{(0)\ell j})^6} + \frac{6\delta_{(2)\ell j}\delta_{(4)\ell j}}{(n - \delta_{(0)\ell j})^7} + \frac{\delta_{(8)\ell j}}{(n - \delta_{(0)\ell j})^8} \\ + \frac{4\delta_{(4)\ell j}^2 + 8\delta_{(2)\ell j}\delta_{(6)\ell j}}{(n - \delta_{(0)\ell j})^9} + \frac{\delta_{(10)\ell j}}{(n - \delta_{(0)\ell j})^{10}} + \frac{-40\delta_{(2)\ell j}^4 + 10\delta_{(4)\ell j}\delta_{(6)\ell j} + 10\delta_{(2)\ell j}\delta_{(8)\ell j}}{(n - \delta_{(0)\ell j})^{11}} + \dots \quad (10)$$

where ℓ and j are the orbital and total electronic angular quantum numbers, respectively².

The input masses of the electron, proton, and deuteron depend on the atomic mass unit, u . At present, the best determination of u comes from the rubidium recoil experiment of Ref [19]; relevant mass-related values are given in Table II. We consider excitation transitions, written in spectroscopic notation, $[n\ell_j]_i \rightarrow [n\ell_j]_f$; the frequencies ($\Delta\nu$) that correspond to these transitions are fit with the equation

$$h\Delta\nu = E_{n_f\ell_f j_f} - \begin{cases} E_0 & (n_i = 1) \\ E_{n_i\ell_i j_i} & (n_i \neq 1) \end{cases} \quad (11)$$

where $E_{n\ell j}$ is the term energy defined in equation (8), E_0 is the ground state energy, the magnitude of which is the ground state ionization energy, E_I .

For each data fitting, we use the Levenburg-Marquardt algorithm, weighting each transition interval by the inverse-square of its measurement uncertainty. The statistical analyses completed for this article were performed using the software *Mathematica* and are included in a publicly available notebook [24].

TABLE II. Mass-related parameters

Quantity	Value	Reference
$h/m(^{87}\text{Rb})$	$4.591\,359\,258\,90(65) \times 10^{-9} \text{ m}^2 \text{ s}^{-1}$	[19]
$m(^{87}\text{Rb})$	$86.909\,180\,53\,10(60) u$	[17]
$m(e)$	$5.485\,799\,090\,65(16) \times 10^{-4} u$	[25]
$m(p)$	$1.007\,276\,466\,583(32) u$	[26]
$m(d)$	$2.013\,553\,212\,535(17) u$	[27]

² Neither the total spin or total system angular momentum quantum number, s or f , are here included because the hyperfine structure of most levels of hydrogen and deuterium has not been resolved.

verify that, at lowest order in $Z\alpha/n_*$, equation (8) is equivalent to equation (2). The standard defect ansatz is to posit that it admits a series expansion in energy, but the following *modified* ansatz was shown to be equivalent and is significantly easier to use for data fitting

B. Model Selection and Multi-model inference

The modified defect series, equation (10), must be truncated at some order for data analysis, therefore each choice of truncation represents a different model. In this article we only consider variations in truncation based on the angular momentum value, ℓ ; however, in the future, additional truncation choices should be considered, e.g., depending on j . At lowest order ($O_\ell = 0$) only the defect parameter $\delta_{(0)\ell j}$ is included, at next-to-lowest order ($O_\ell = 1$) both $\delta_{(0)\ell j}$ and $\delta_{(2)\ell j}$ are included, and so on. There is no obvious place to truncate the series, and there may not be one, hence there are multiple (nested) models to consider, implying a *model selection uncertainty*. There are at least two distinct reasons for this. First, given ever-present experimental uncertainties, parsimony is a guiding principle in model selection which attempts to optimize for the inherent tradeoff between bias and parameter variance; too few parameters can result in significant bias and an overestimate of precision, while too many parameters can result in higher variance [28]. Finding the right balance requires care, as described in the paragraphs below.

The second reason for model selection uncertainty is because of the asymptotic foundation of the relativistic Ritz model. At the present time, it is not known if the series in equation (10) converges, so it is for now conservatively assumed to be an asymptotic series. Such series are known to have an optimal point of truncation beyond which the approximation becomes less accurate; in fact, the series may diverge. However, useful information may be contained within *all* terms of such a series [29], suggesting that analysis of models with more than the optimal number of parameters may be fruitful.

Ref [28] contains an excellent discussion of the use of the so-called second-order Akaike information criterion (AICc) for comparing the goodness-of-fit of various models to a given data set. This information-theoretic criterion, a quantity that estimates the relative Kullback-

Leibler entropy, is defined by

$$\text{AICc}_i = -2 \log \mathcal{L}(\hat{\theta}_i) + 2K_i \left(\frac{N}{N - K_i - 1} \right), \quad (12)$$

where $\mathcal{L}(\hat{\theta}_i)$ is the maximum likelihood function, conditional on model i , for the set of best-fit model parameters, $\hat{\theta}_i$, N is the sample size, and K_i is the number of parameters in model i . AICc, as opposed to Akaike's original AIC, is used whenever the data set is not sufficiently large; the rule of thumb is that AICc should be used whenever $N/K_i < 40$ [28].

The “best” model has the minimum value of AICc; however, the magnitudes of the AICc values are by themselves not meaningful. What matters is the AICc differences, defined by

$$\Delta_i \equiv \text{AICc}_i - \text{AICc}_{\min}, \quad (13)$$

and the *evidence* of model i depends exponentially on Δ_i , namely it is proportional to $\exp(-\frac{1}{2}\Delta_i)$. However, it is often the case that many models fit to the same data will yield AICc values near to AICc_{\min} , perhaps within 0 to 2 units, suggesting that the “best” model may well vary – sheerly by chance – on a particular realization of data. In other words, if all data was re-collected and re-fit the AICc values would change and the best fit model may differ. Wanting to draw robust conclusions from a single existing data set, therefore, leads us to average across multiple models. For this purpose, the *Akaike weights* for model i are introduced;

$$w_i = \frac{e^{-\frac{1}{2}\Delta_i}}{\sum_{j=1}^R e^{-\frac{1}{2}\Delta_j}}, \quad (14)$$

where R is the number of models under consideration. Note that by definition the Akaike weights sum to unity. The value of generic model parameter θ_a will have a best estimate, conditional on model i , denoted here by $\hat{\theta}_{a,i}$. The model-averaged estimate for θ_a is

$$\langle \hat{\theta}_a \rangle = \sum_{i=1}^R w_i \hat{\theta}_{a,i}. \quad (15)$$

Finally, we should seek an estimate of the error in (15) that is not conditional on a particular model, hence referred to as an *unconditional* error estimate. The procedure described in [28] includes both the conditional variance estimate, $\widehat{\text{var}}(\hat{\theta}_{a,i})$, and a “variance component” due to the fluctuation of the conditional parameter value around its model average, $(\hat{\theta}_{a,i} - \langle \hat{\theta}_a \rangle)^2$. The estimate of the unconditional standard error (se) is given by

$$\text{se}(\hat{\theta}_a) = \sum_{i=1}^R w_i \sqrt{\widehat{\text{var}}(\hat{\theta}_{a,i}) + (\hat{\theta}_{a,i} - \langle \hat{\theta}_a \rangle)^2}. \quad (16)$$

Given the uncertainty inherent to model selection, as well as the psychological dangers associated with data analysis, e.g. data dredging, we proceed cautiously with several exploratory analyses involving subsets of hydrogen and deuterium transitions described in the sections below.

III. ATOMIC HYDROGEN

The data used here are primarily found in the NIST Atomic Spectral Database (ASD) [12], which uses the 2010 hydrogen compilation [11]. We make two updates, replacing the $2S_{1/2} \rightarrow 8D_{5/2}$ transition with that from the more recent measurement of Ref. [30] and adding the $1S_{1/2} \rightarrow 3S_{1/2}$ transition measurement from Ref. [31]. The ASD $2S_{1/2} \rightarrow 6S_{1/2}$ & $2S_{1/2} \rightarrow 6D_{5/2}$ transitions are omitted from analysis, as they had not been directly observed³ at the time the 2010 compilation was published. As described in the line references in the ASD table, many lines identified as “observed” are, in fact, only interpolations or extrapolations of measured transitions using the non-relativistic Ritz procedure, i.e. using (2); all such data are also omitted from analysis. The full list of transitions considered are shown in Tables VII and VIII.

It is also important to emphasize what we fit here are the fine-structure transitions, i.e., without explicit consideration of interactions that involve the nuclear spin. However, many measurements require theoretical corrections to obtain the corresponding fine-structure transition. In this sense, the data used here generally represent a combination of experimental results with statistical mechanical and bound-state QED theory corrections.

A. Exploratory hydrogen analysis: $S_{1/2}$ & $D_{5/2}$ states

Here we consider only the transitions between the $S_{1/2}$ and $D_{5/2}$ states, of which there are only 10 measurements, summarized below in Table III. The relativistic Ritz model at various points of truncation of the modified defect (equation (10)) are labeled $\text{RR}O_S O_D$. A selection of models were fit to this data and the AICc differences, Δ_i , are reported in Table IV. Given the exponential dependence of the relative evidence on Δ_i , model RR10 – a next-to-lowest order fit for S states and a lowest order fit for D states – is by far the best. The parameter fits from the RR10 model analysis are reported in Table V. Note that there are significant correlations amongst the

³ As explained in Ref. [11], those data reported in Ref. [12] had only been determined from a combination of other measurements and from the (nonrelativistic) Ritz value of the $1S_{1/2} \rightarrow 3S_{1/2}$ frequency. I thank Alexander Kramida for clarifying this point.

model parameters, which are quantified in the correlation matrix shown in Table VI.

TABLE III. List of hydrogen transition data used for exploratory fitting. Alternate references are given for data taken from other than the compilation in Ref. [12].

Number	Transition	Frequency (GHz)
1	$1S_{1/2} \rightarrow 3S_{1/2}$	2 922 743.278 665 79(72) [31]
2	$1S_{1/2} \rightarrow 2S_{1/2}$	2 466 061.413 187 070(30)
3	$2S_{1/2} \rightarrow 12D_{5/2}$	799 191.727 4038(64)
4	$2S_{1/2} \rightarrow 10D_{5/2}$	789 144.886 412(39)
5	$2S_{1/2} \rightarrow 8D_{5/2}$	770 649.561 5709(20) [30]
6	$2S_{1/2} \rightarrow 8S_{1/2}$	770 649.350 0121(99)
7	$2S_{1/2} \rightarrow 4D_{5/2}$	616 521.843 441(24)
8	$2S_{1/2} \rightarrow 4S_{1/2}$	616 520.150 637(10)
9	$3S_{1/2} \rightarrow 3D_{5/2}$	4.013 162(48)
10	$4S_{1/2} \rightarrow 4D_{5/2}$	1.692 98(38)

TABLE IV. Second-order Akaike information criterion differences, Δ_i , for the exploratory analysis of $S_{1/2} \rightarrow S_{1/2}$ & $D_{5/2}$ transitions.

O_S	O_D			
	0 (LO)	1 (NLO)	2 (NNLO)	3 (N ³ LO)
0 (LO)	35.5	47.2	78.3	162.
1 (NLO)	0	27.5	106.	∞
2 (NNLO)	15.8	90.4	∞	∞
3 (N ³ LO)	108.	∞	∞	–

TABLE V. Fit parameters for model RR10 used in the exploratory analysis.

$\delta_{(0)0\frac{1}{2}}$	$2.5344(1) \times 10^{-5}$
$\delta_{(2)0\frac{1}{2}}$	$4.8(2) \times 10^{-8}$
$\delta_{(0)2\frac{5}{2}}$	$8.8724(9) \times 10^{-6}$
$E_0^{(H)}$ [eV]	-13.598 434 599 543(73)
α^{-1}	137.035 999 298(38)

TABLE VI. Correlation Matrix for the RR10 model in the exploratory analysis.

	$\delta_{(0)0\frac{1}{2}}$	$\delta_{(2)0\frac{1}{2}}$	$\delta_{(0)2\frac{5}{2}}$	E_0	α^{-1}
$\delta_{(0)0\frac{1}{2}}$	1				
$\delta_{(2)0\frac{1}{2}}$	-0.996	1			
$\delta_{(0)2\frac{5}{2}}$	0.9612	-0.9657	1		
E_0	0.9558	-0.9474	0.8645	1	
α^{-1}	0.9995	-0.9980	0.9550	0.9646	1

As a check of the conditional sampling error estimates in Table V, we perform a bootstrap analysis, resampling and replacing each of the 10 transition measurements with a random value drawn from a normal distribution whose mean is the measured value and standard deviation is equal to the measurement uncertainty.

Ten thousand ($B = 10,000$) such re-samplings were performed and analyzed with the RR10 model, the results of which give standard deviations $\sigma_{E_0} = 4.3 \times 10^{-10}$ eV and $\sigma_{\alpha^{-1}} = 2.2 \times 10^{-8}$, in reasonable agreement with the conditional sampling error estimates shown in Table V.

In addition to these statistical considerations, the mass-related inputs (Table II) have uncertainties that must be propagated. To account for this, we perform a Monte Carlo analysis, resampling and replacing each of the 4 mass-related measurements with a random value drawn from a normal distribution whose mean and standard deviation are given by its measured value and uncertainty, respectively. Ten thousand ($B = 10,000$) such re-samplings were performed and analyzed with the RR10 model, giving standard deviations $\sigma_{E_0} \leq 10^{-16}$ eV (negligible) and $\sigma_{\alpha^{-1}} = 1.1 \times 10^{-8}$. The latter value is, not coincidentally, equal to the uncertainty in $\sigma_{\alpha^{-1}}$ claimed by the authors of Ref. [19].

Finally, from this exploratory analysis

$$\begin{aligned} \alpha^{-1} &= 137.035\,999\,298(38)_{\text{data}}(11)_{\text{mass}} \\ &= 137.035\,999\,298(40) \end{aligned} \quad (17)$$

where the subscript “data” denotes the statistical uncertainty due to transition data fitting and model averaging and “mass” denotes uncertainty due to uncertainty in the mass-related inputs. The ionization energy of hydrogen from this analysis is

$$E_I^{(H)} = 13.598\,434\,599\,543(73) \text{ eV}. \quad (18)$$

There is a discrepancy of approximately $\simeq 2.5\sigma$ between (17) and (18) and their expected values in Table I and equation (5), respectively. Notably, our determination of α^{-1} here is systematically too high, but this is expected. When fewer parameters are used α^{-1} will be biased toward larger values, as found in the theoretical analysis in Ref [8]. Through the inclusion of more transitions, it becomes feasible that models with more parameters are favored, thus leading to a more reliable determination of α and E_I . We address this in the following subsections.

B. Initial hydrogen $S, P,$ & D -channel analysis

Here we analyze the 60 measured hydrogen transitions coming primarily the NIST ASD 2010 hydrogen compilation [12], which includes all transitions between the 5 angular momentum channels $S_{1/2}, P_{1/2}, P_{3/2}, D_{3/2},$ and $D_{5/2}$. These data are summarized in Tables VII and VIII. A selection of AICc differences are given in Tables IX, X, and XI.

TABLE IX. Second-order Akaike information criterion differences, Δ_i , for the initial analysis of S , P , and D -channel transitions in hydrogen. Here $O_D = 0$. Bolded values identify the models used for averaging.

O_S	O_P				
	0	1	2	3	4
0	368.8	257.2	261.7	268.9	276.8
1	30.1	13.1	17.5	24.8	33.1
2	32.9	0.	3.6	11.2	19.9
3	35.6	3.5	7.5	15.5	24.6
4	38.1	5.5	9.7	18.1	27.7

TABLE X. Second-order Akaike information criterion differences, Δ_i , for the initial analysis of S , P , and D -channel transitions in hydrogen. Here $O_D = 1$. Bolded values identify the models used for averaging.

O_S	O_P				
	0	1	2	3	4
0	374.3	236.6	239.6	247.5	256.3
1	19.2	14.0	18.7	26.8	35.9
2	22.4	5.3	7.0	15.4	25.0
3	25.5	9.0	10.6	19.5	29.6
4	28.0	11.3	13.1	22.4	33.1

TABLE XI. Second-order Akaike information criterion differences, Δ_i , for the initial analysis of S , P , and D -channel transitions in hydrogen. Here $O_D = 2$.

O_S	O_P				
	0	1	2	3	4
0	379.4	240.9	244.2	252.9	262.6
1	14.6	8.2	12.8	21.7	31.8
2	16.3	8.1	11.5	21.0	31.7
3	13.7	10.9	16.1	26.1	37.4
4	16.1	13.4	19.1	29.5	41.4

Despite the well-established procedures for model averaging and error estimation described in Section II B, there is still freedom in the decision of which models to include in this analysis. At the very least, it would seem that model RR210 should be included in the average, but what others? Models RR220 and RR310 have only moderately large AICc differences, so they should also be included. Considering that this would represent a kind of exploration in the number of S - and P -channel defect parameters, it seems prudent to also consider model RR320, as well as a variation in the number of D -state parameters. For this reason, we also include models RR211, RR221, RR311, and RR321. *This creates a contiguous and compact exploration of the (O_S, O_P, O_D) parameter space.* These 8 models are identified with bold text in Tables IX and X. The Akaike weights for the set of these

8 models, along with a selection of parameter values are summarized in Table XII.

TABLE XII. Akaike weights and some parameter fits for the initial (uncut) hydrogen S , P , and D -channel analysis.

Model	w_i	α^{-1}	$E_I^{(H)}$ eV
RR210	0.6774	137.035 999 248(21)	13.598 434 599 625(38)
RR220	0.1100	137.035 999 246(22)	13.598 434 599 630(39)
RR310	0.1178	137.035 999 248(22)	13.598 434 599 626(40)
RR320	0.0161	137.035 999 245(22)	13.598 434 599 631(40)
RR211	0.0475	137.035 999 207(40)	13.598 434 599 659(48)
RR221	0.0203	137.035 999 170(46)	13.598 434 599 697(53)
RR311	0.0075	137.035 999 203(42)	13.598 434 599 660(48)
RR321	0.0033	137.035 999 160(49)	13.598 434 599 702(54)

Going through the model averaging and uncertainty analysis described in Section II B, we determine

$$\begin{aligned} \alpha^{-1} &= 137.035\,999\,244(25)_{\text{data}}(11)_{\text{mass}} \\ &= 137.035\,999\,244(27), \end{aligned} \quad (19)$$

which is approximately 1.5σ discrepant from the consensus of values in I. The hydrogen ground state ionization energy is simultaneously determined to be

$$E_I^{(H)} = 13.598\,434\,599\,629(41)\text{ eV}, \quad (20)$$

which is approximately 1.5σ discrepant from the Standard Model prediction in equation (5).

It is at this point worth evaluating some measure of goodness-of-fit. This is done by considering the fit residuals, defining the residual of the i 'th transition as

$$\varepsilon_i = \Delta\nu_{\text{measured},i} - \Delta\nu_{\text{model},i}. \quad (21)$$

One approach would be to consider these residuals normalized to the measurement uncertainty of each transition. Doing so results in a mean of -0.126 and a standard deviation of 0.787 . Another option is to consider the so-called standardized residuals, defined to have a mean of 0 and standard deviation equal to unity. The advantage of the standardized residuals is that they take into account the leverage of each data point, making data that deviate from the model prediction stand out when those data have a larger influence on the fit. The standardized residuals from the RR210 fit are shown in Figure 1. For every model, the transition $2S_{1/2} \rightarrow 3P_{1/2}$ stands out as significantly discrepant; in all models the standardized residual for this datum is lower than -3.0 . Although such discrepancies are expected to occur due to random measurement error, a discrepancy at or exceeding 3σ is expected with an occurrence of 0.3% , or an average of only 0.18 out of 60 . The anomalous nature of this data point warrants another analysis with it removed, which we do in the following section.

All workers following this approach are advised to be both cautious when pursuing such investigations and transparent about their methodologies when publicizing their results.

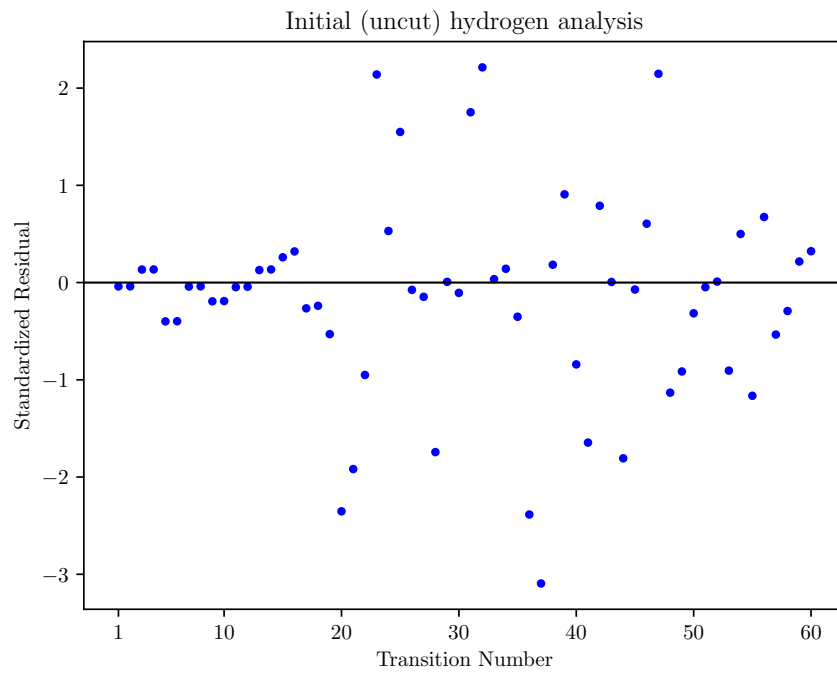


FIG. 1. Standardized residuals from the initial (uncut) hydrogen analysis. Transitions identified in Tables VII and VIII.

C. Hydrogen analysis without $2S_{1/2} \rightarrow 3P_{1/2}$

Here we repeat the analysis of Section III B without the $2S_{1/2} \rightarrow 3P_{1/2}$ transition. The 8 best models remain the same as in the previous section. The Akaike weights and some parameter values are given in Table XIII.

TABLE XIII. Akaike weights and some parameter fits for the hydrogen S , P , and D -channel analysis, removing the $2S_{1/2} \rightarrow 3P_{1/2}$ transition.

Model	w_i	α^{-1}	$E_I^{(H)}$ eV
RR210	0.6041	137.035 999 246(19)	13.598 434 599 629(35)
RR220	0.1306	137.035 999 246(19)	13.598 434 599 630(35)
RR310	0.1036	137.035 999 246(20)	13.598 434 599 630(36)
RR320	0.0187	137.035 999 245(20)	13.598 434 599 631(36)
RR211	0.0821	137.035 999 197(36)	13.598 434 599 670(43)
RR221	0.0402	137.035 999 170(41)	13.598 434 599 697(47)
RR311	0.0138	137.035 999 192(37)	13.598 434 599 671(43)
RR321	0.0070	137.035 999 160(43)	13.598 434 599 702(48)

Performing the averaging and uncertainty analysis again, we determine

$$\begin{aligned} \alpha^{-1} &= 137.035\,999\,238(27)_{\text{data}}(11)_{\text{mass}} \\ &= 137.035\,999\,244(29), \end{aligned} \quad (22)$$

and

$$E_I^{(H)} = 13.598\,434\,599\,636(40)\text{ eV}, \quad (23)$$

the latter of which is a marginal improvement over the results from the previous section. However, the standardized residuals, which are shown in Figure 2, show that both the $2S_{1/2} \rightarrow 3P_{3/2}$ and $1S_{1/2} \rightarrow 3P_{3/2}$ transitions are discrepant at about 2.6σ . Again, this is statistically unlikely to occur with only 59 data points and motivates their removal in another re-analysis.

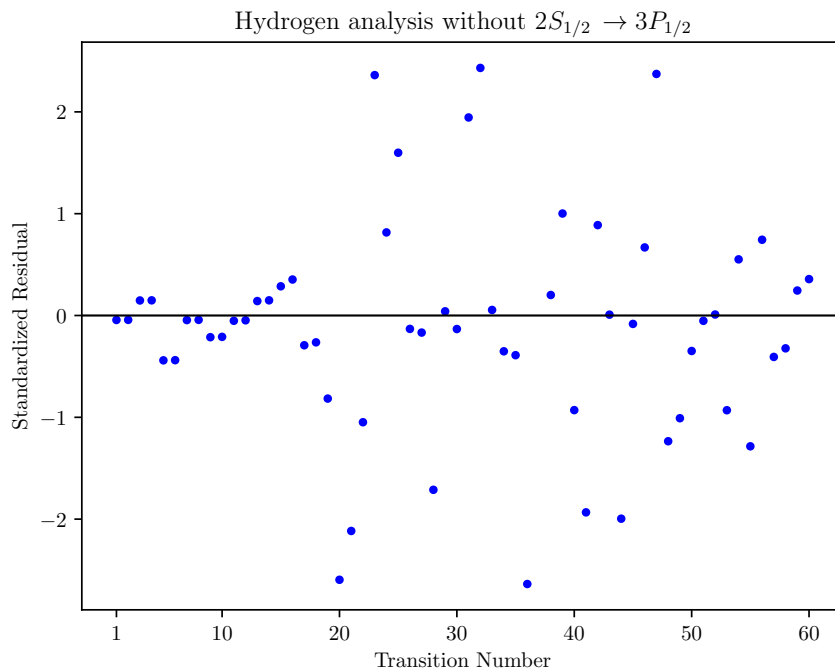


FIG. 2. Standardized residuals from the hydrogen analysis omitting the $2S_{1/2} \rightarrow 3P_{1/2}$ transition. Transitions identified in Tables VII and VIII.

D. Hydrogen analysis with multiple cuts

We continue making cuts of one to two transitions until the standardized residuals indicate no substantially outlying data. In total, this requires cutting the transitions $1S_{1/2} \rightarrow 3P_{3/2}$, $1S_{1/2} \rightarrow 3P_{1/2}$, $1S_{1/2} \rightarrow 2P_{1/2}$, $2S_{1/2} \rightarrow 3P_{3/2}$, $2S_{1/2} \rightarrow 3P_{1/2}$, $3S_{1/2} \rightarrow 3P_{3/2}$, and $4P_{1/2} \rightarrow 4D_{3/2}$, which corresponds to transitions 20, 21, 23, 36, 37, 44, and 47 in Tables VII and VIII. AICc differences are given in Tables XV through XVII, choosing RR211 as the best model. Although the minimum AICc value suggests that RR411 is naively the best, the principle of parsimony and an expectation that *over-fitting* is possible suggests that the model with the local AICc minimum closest to RR000 should be chosen as the best, which is RR211. The parameter fits for RR211 are given in Table XIV and some of the AICc differences are given in Tables XV, XVI, and XVII. The Akaike weights and some parameter values are given in Table XVIII and the standardized residuals are shown in Figure 3.

TABLE XIV. Fit parameters for hydrogen with RR211.

$\delta_{(0)0\frac{1}{2}}$	$2.53392(7) \times 10^{-5}$
$\delta_{(2)0\frac{1}{2}}$	$7.9(4) \times 10^{-8}$
$\delta_{(4)0\frac{1}{2}}$	$-7.0(9) \times 10^{-8}$
$\delta_{(0)1\frac{1}{2}}$	$2.66381(6) \times 10^{-5}$
$\delta_{(2)1\frac{1}{2}}$	$1.3(1) \times 10^{-8}$
$\delta_{(0)1\frac{3}{2}}$	$1.32944(6) \times 10^{-5}$
$\delta_{(2)1\frac{3}{2}}$	$1.2(1) \times 10^{-8}$
$\delta_{(0)2\frac{3}{2}}$	$1.33157(8) \times 10^{-5}$
$\delta_{(2)2\frac{3}{2}}$	$2(1) \times 10^{-8}$
$\delta_{(0)2\frac{5}{2}}$	$8.8684(8) \times 10^{-6}$
$\delta_{(2)2\frac{5}{2}}$	$1.4(4) \times 10^{-8}$
E_0 [eV]	-13.598 434 599 682(23)
α^{-1}	137.035 999 186(19)

TABLE XV. Second-order Akaike information criterion differences, Δ_i , for the S , P , and D -channel analysis in hydrogen with multiple transition cuts. Here $O_D = 0$.

O_S	O_P				
	0	1	2	3	4
0	404.8	307.3	312.4	320.2	329.0
1	84.14	49.22	54.19	62.00	71.15
2	87.01	7.167	11.62	19.21	28.72
3	89.81	10.88	15.80	23.92	34.04
4	92.23	8.552	13.56	21.56	32.30

TABLE XVI. Second-order Akaike information criterion differences, Δ_i , as in Table XV. Here $O_D = 1$. Bolded values identify the models used for averaging.

O_S	O_P				
	0	1	2	3	4
0	410.7	290.2	294.0	302.8	312.6
1	65.00	45.38	48.43	57.09	67.39
2	68.20	0	3.490	11.74	22.40
3	71.32	2.542	5.411	14.20	25.55
4	73.39	-1.831	0.4025	8.641	20.67

TABLE XVII. Second-order Akaike information criterion differences, Δ_i , as in Table XV. Here $O_D = 2$. Bolded values identify the models used for averaging.

O_S	O_P				
	0	1	2	3	4
0	416.0	294.2	298.5	308.4	319.5
1	53.42	25.63	23.03	32.28	43.79
2	54.16	3.172	9.333	18.88	31.02
3	47.69	7.764	14.31	24.72	37.75
4	48.56	3.154	9.869	19.61	33.46

TABLE XVIII. Akaike weights and parameters from the hydrogen S , P , and D -channel analysis with multiple transition cuts.

Model	w_i	α^{-1}	$E_I^{(H)}$ eV
RR211	0.5690	137.035 999 186(19)	13.598 434 599 682(23)
RR221	0.0994	137.035 999 171(22)	13.598 434 599 697(25)
RR311	0.1596	137.035 999 180(20)	13.598 434 599 683(23)
RR321	0.0380	137.035 999 162(23)	13.598 434 599 701(25)
RR212	0.1165	137.035 999 206(24)	13.598 434 599 682(25)
RR222	0.0053	137.035 999 197(34)	13.598 434 599 690(31)
RR312	0.0117	137.035 999 214(31)	13.598 434 599 681(25)
RR322	0.0004	137.035 9984(14)	13.598 434 600 10(77)

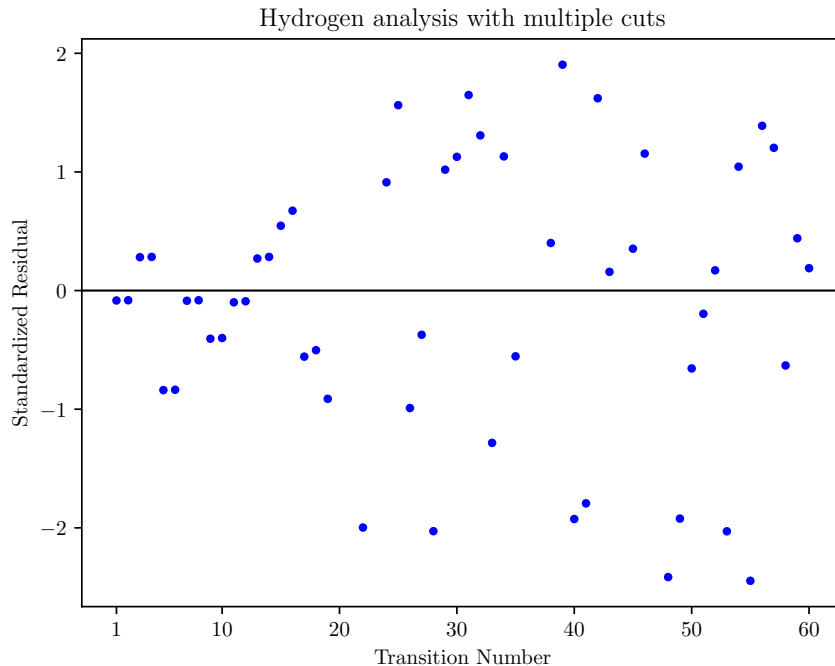


FIG. 3. Standardized residuals from the hydrogen analysis omitting several transitions; see text for details. Transitions identified in Tables VII and VIII.

Here we repeat the analysis of Section III B and III C. We determine

$$\begin{aligned}\alpha^{-1} &= 137.035\,999\,185(23)_{\text{data}}(11)_{\text{mass}} \\ &= 137.035\,999\,185(25),\end{aligned}\quad (24)$$

which is in agreement with the values in Table I at the level of 1.8×10^{-10} , with the exception of Ref. [16]; as described in Section III F below, the discrepancy here can be attributed to a discrepant determination of the atomic mass unit, u . At the same time, we find

$$E_I^{(\text{H})} = 13.598\,434\,599\,684(25)\text{ eV},\quad (25)$$

which is in agreement with the Standard Model prediction (5) at the level of 1.8×10^{-12} . As part of this agreement, additional confirmation is possible for recent determinations of the proton radius, of particular interest given the so-called proton radius puzzle [32]. Consider that the leading order nuclear size correction to the hydrogen ground state energy is

$$\Delta E_{\text{NS}}(r_p) = \frac{8\pi^2}{3}\alpha^4 m_{\text{red}}^3 r_p^2 = 6.5 \times 10^{-9}\text{ eV} \left(\frac{r_p}{1\text{ fm}}\right)^2,\quad (26)$$

whereas the next-to-leading order correction is about 10^{-4} times smaller [33]. This means that a variation

in the proton radius would vary the ground state energy by approximately

$$\delta\Delta E_{\text{NS}}(r_p) \simeq 1.1 \times 10^{-10}\text{ eV} \left(\frac{r_p}{0.84\text{ fm}}\right) \left(\frac{\delta r_p}{0.01\text{ fm}}\right),\quad (27)$$

where $r_p \simeq 0.84\text{ fm}$ is the currently accepted value [10]. An error of $\delta r_p = 0.04\text{ fm}$, corresponding to the older (incorrect) value of $r_p \simeq 0.88\text{ fm}$, would have likely resulted in disagreement between the Standard Model value (5) and the data-driven value in (25). This suggests a path toward further testing of nuclear structure models.

Finally, we can make contact with other analyses of hydrogen transition data by using this analysis to make a BSQED-independent determination of the Rydberg constant,

$$R_\infty = \frac{1}{2} \frac{m_e c}{h} \alpha^2.\quad (28)$$

To find its uncertainty we must consider the effect of the statistical uncertainty (due to fitting) as well as the uncertainty propagated from the mass-related input parameters. The latter are found to be sub-dominant to the former, which amount to $3.7 \times 10^{-3}\text{ m}^{-1}$. Therefore, this analysis gives

$$R_\infty = 10\,973\,731.5718(37)\text{ m}^{-1}.\quad (29)$$

which is in agreement at the level of 3.4×10^{-10} with the value as determined using BSQED analyses of specific atomic transitions [10].

E. Predictions for omitted transitions

Using the fits from Section III D, here we predict values for the 7 transitions omitted from that analysis. Predictions for a particular transition can be written in the form

$$\Delta\nu = f(\Theta), \quad (30)$$

where f represents $1/h$ times the right hand side of equation (11) and Θ is the vector of best-fit parameters from a particular fit. The uncertainty in $\Delta\nu$, $\sigma_{\Delta\nu}$ is given by

$$\sigma_{\Delta\nu}^2 = \mathbf{g}^T \mathcal{C} \mathbf{g} \quad (31)$$

where the components of the vector \mathbf{g} are

$$\mathbf{g}_a = \frac{\partial f}{\partial \Theta_a} \quad (32)$$

and the covariance matrix has components

$$\mathcal{C}_{ab} = \text{cov}(\Theta_a, \Theta_b), \quad (33)$$

both of which can be easily obtained with software, such as *Mathematica*.

As an illustration, the main points of the analysis using the RR211 model on the transition $2S_{1/2} \rightarrow 3P_{1/2}$ are summarized here. With the best-fit parameters for that model, given in Table XIV, equation (11) predicts

$$\Delta\nu(2S_{1/2} \rightarrow 3P_{1/2})_{\text{RR211}} = 456\,681\,550\,679 \text{ kHz}. \quad (34)$$

We take the components of \mathbf{g} to be listed in the same order as that of Table XIV. Taking the derivatives of $f(\Theta)_{\text{RR211}}$ with respect to those parameters and evaluating with the best-fit values,

$$\mathbf{g} = \begin{pmatrix} 27\,420 \\ 6\,855 \\ 1\,714 \\ -8\,124 \\ -903 \\ 0 \\ 0 \\ 0 \\ 0 \\ 0 \\ 0 \\ 0 \\ 0 \\ -222 \end{pmatrix} \text{ kHz}, \quad (35)$$

where each zero indicates that a parameter has no effect on the prediction for this particular transition.

The covariance matrix output by the fitting software is omitted here for brevity. The result for the error estimate using (31) is

$$(\sigma_{\Delta\nu})_{\text{RR211}} = 14 \text{ kHz}. \quad (36)$$

The same procedure is followed for the remaining 7 models; a summary of results is given in Table XIX. A weighted average may be computed along with an unconditional error estimate, determined following the procedure described in Section III A.

TABLE XIX. Akaike weights and predictions for the $2S_{1/2} \rightarrow 3P_{1/2}$ transition.

Model	w_i	$\Delta\nu$ [kHz]
RR211	0.5690	456 681 550 679(14)
RR221	0.0994	456 681 550 659(20)
RR311	0.1596	456 681 550 682(14)
RR321	0.0380	456 681 550 659(20)
RR212	0.1165	456 681 550 665(16)
RR222	0.0053	456 681 550 659(20)
RR312	0.0117	456 681 550 660(20)
RR322	0.0004	456 681 550 659(20)

The final model-averaged prediction is

$$\Delta\nu(2S_{1/2} \rightarrow 3P_{1/2})_{\text{RR}} = 456\,681\,550\,675(17) \text{ kHz}. \quad (37)$$

which should be compared with the ASD 2010 value

$$\Delta\nu(2S_{1/2} \rightarrow 3P_{1/2})_{\text{ASD}} = 456\,681\,549\,89(28) \text{ kHz}, \quad (38)$$

which originates in the measurement of Ref. [34]. The measured value in (38) is smaller than the relativistic Ritz prediction (37) by approximately 2.8σ , yet (37) is more than an order of magnitude more precise than the measurement. A new measurement of this transition frequency would be an excellent test of the overall approach presented here. The complete set of predictions for all 7 of the omitted transitions may be found in Table XX.

TABLE XX. Predictions of omitted transition frequencies in the hydrogen S , P , and D -channel analysis. The last column is the non-relativistic Ritz interpolation using equation (2).

Transition	Rel. Ritz [GHz]	ASD Measured [GHz]	ASD NR Ritz [GHz]
$\Delta\nu(2S_{1/2} \rightarrow 3P_{1/2})$	456 681.550 675(17)	456 681.549 89(28)	456 681.549 96(21)
$\Delta\nu(2S_{1/2} \rightarrow 3P_{3/2})$	456 684.800 756(60)	456 684.800 11(28)	456 684.800 04(21)
$\Delta\nu(1S_{1/2} \rightarrow 3P_{1/2})$	2 922 742.963 862(17)	2 922 728.6(8.6)	2 922 742.9632(2)
$\Delta\nu(1S_{1/2} \rightarrow 3P_{3/2})$	2 922 746.213 943(60)	2 922 728.6(8.6)	2 922 746.2132(2)
$\Delta\nu(1S_{1/2} \rightarrow 2P_{1/2})$	2 466 060.355 3394(37)	2 466 068.0(4.1)	2 466 060.355 3404(81)
$\Delta\nu(3S_{1/2} \rightarrow 3P_{3/2})$	2.935 277(60)	2.9334(12)	2.935 268(60)
$\Delta\nu(4P_{1/2} \rightarrow 4D_{3/2})$	1.3689(13)	1.3711(12)	1.369 10(25)

F. Effect of variation in the atomic mass unit

There is by now a known discrepancy in the determined value of the fine-structure constant from two different groups, [16] and [19], based on their measurements of the absolute masses of rubidium and cesium, respectively. Consider then, swapping the role played by the rubidium values in Table II for those given in Table XXI.

TABLE XXI. Mass-related parameters

Quantity	Value	Reference
$h/m(^{133}\text{Cs})$	$3.002\,369\,4721(12) \times 10^{-9} \text{ m}^2 \text{ s}^{-1}$	[16]
$m(^{133}\text{Cs})$	$86.909\,180\,53\,10(60) u$	[17]

Here we repeat the analysis of Section III D, performing the averaging and uncertainty analysis yet again. We determine

$$\begin{aligned} \alpha^{-1} &= 137.035\,999\,025(23)_{\text{data}}(28)_{\text{mass}} \\ &= 137.035\,999\,025(36), \end{aligned} \quad (39)$$

which is in agreement with Ref. [16] but not with any other determination in Table I. At the same time, we find

$$E_I^{(\text{H})} = 13.598\,434\,599\,684(24) \text{ eV}, \quad (40)$$

which is still in agreement with the Standard Model prediction (5) at the level of 1.8×10^{-12} . This may be pertinent because improved determinations of $E_I^{(\text{H})}$ should be possible with new and/or improved spectroscopic data even without improvement in the determination of the amu or, likewise, a consensus between the authors of [16] and [19] on its value.

G. Hydrogen analysis with fixed α

Here we fix the value $\alpha^{-1} = 137.035\,999\,166(15)$, obtained recently through an improved measurement of the

electron g -factor [18] and repeat the analysis of the 7 transition frequency cuts described in Section III D. The Akaike weights and ionization energies are reported in Table XXII.

TABLE XXII. Akaike weights and ionization energy fits for the hydrogen S , P , and D -channel analysis with fixed α from Ref. [18].

Model	w_i	$E_I^{(\text{H})} \text{ eV}$
RR211	0.4632	13.598 434 599 7033(91)
RR221	0.1968	13.598 434 599 7023(88)
RR311	0.2028	13.598 434 599 6981(98)
RR321	0.0878	13.598 434 599 6969(94)
RR212	0.0348	13.598 434 599 718(14)
RR222	0.0080	13.598 434 599 715(13)
RR312	0.0054	13.598 434 599 710(17)
RR322	0.0012	13.598 434 599 706(17)

The measurement error in α^{-1} leads to a variation in the energy of 1.5×10^{-11} eV. Altogether,

$$\begin{aligned} E_I^{(\text{H})} &= 13.598\,434\,599\,702(10)_{\text{data}}(15)_{\alpha} \text{ eV} \\ &= 13.598\,434\,599\,702(18) \text{ eV}, \end{aligned} \quad (41)$$

which is a marginal improvement to (25), the value obtained in the variable- α analysis, and in agreement with the Standard Model prediction (5) at the level of 1.3×10^{-12} .

IV. ATOMIC DEUTERIUM

A. Deuterium with variable α

Here we analyze the 36 measured deuterium transitions from the NIST ASD 2010 hydrogen compilation [12], which includes all transitions between the 5 angular momentum channels $S_{1/2}$, $P_{1/2}$, $P_{3/2}$, $D_{3/2}$, and $D_{5/2}$. These data are summarized in Table XXIII. The fitting

follows as in previous sections, and in particular involves fitting for the fine-structure constant, α . The Akaike weights and some parameter values are given in Table XXIV.

TABLE XXIV. Akaike weights and some parameter fits for the deuterium S , P , and D -channel variable- α analysis.

Model	w_i	α^{-1}	$E_I^{(D)}$ eV
RR100	0.7095	137.035 999 306(29)	13.602 134 636 459(39)
RR110	0.0235	137.035 999 293(33)	13.602 134 636 459(44)
RR200	0.1986	137.035 999 292(31)	13.602 134 636 459(40)
RR210	0.0064	137.035 999 274(36)	13.602 134 636 459(45)
RR101	0.0544	137.035 999 327(33)	13.602 134 636 459(40)
RR111	0.0006	137.035 999 318(42)	13.602 134 636 459(47)
RR201	0.0057	137.035 999 299(58)	13.602 134 636 459(45)
RR211	0.0013	137.035 999 01(14)	13.602 134 636 459(88)

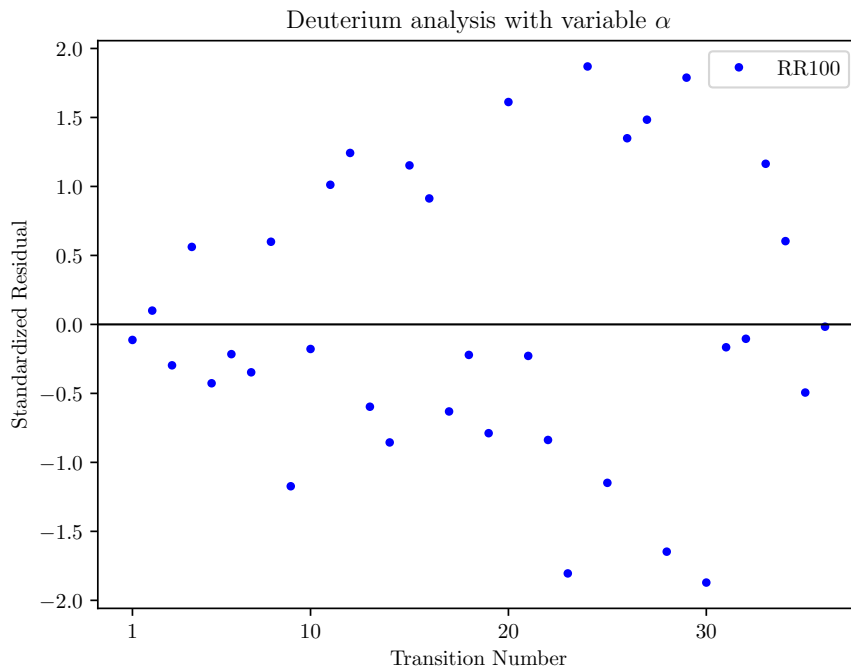


FIG. 4. Standardized residuals from the deuterium analysis performed with variable α . Transitions identified in Table XXIII.

From this initial analysis we determine

$$\begin{aligned} \alpha^{-1} &= 137.035\,999\,303(31)_{\text{data}}(11)_{\text{mass}} \\ &= 137.035\,999\,303(33) \end{aligned} \quad (42)$$

and

$$E_I^{(D)} = 13.602\,134\,636\,461(40) \text{ eV}, \quad (43)$$

The inverse fine-structure constant is far higher than what would be expected based on the values given in Table I, but this is consistent with a preference here for

models with a low number of parameters, as discussed in Section III A.

Standardized residuals are given in Figure 4. There is no obvious outlier data to consider cutting. It appears that, given the relative paucity of deuterium transition data (as compared to hydrogen), it is not possible to make a reliable determination of both the fine-structure constant and deuterium ionization energy.

B. Deuterium with fixed α

In this section we impose a value of the fine structure constant determined in Ref. [18],

$$\alpha^{-1} = 137.035\,999\,166(15), \quad (44)$$

and repeat the analysis from the previous section. The Akaike weights and ionization energies are given in Table XXV.

TABLE XXV. Akaike weights and ionization energies for the deuterium S, P , and D -channel analysis with fixed α .

Model	w_i	$E_I^{(D)}$ eV
RR211	0.7240	13.602 134 636 539(25)
RR201	0.1649	13.602 134 636 541(29)
RR311	0.0455	13.602 134 636 537(26)
RR301	0.0140	13.602 134 636 542(30)
RR210	0.0211	13.602 134 636 612(19)
RR200	0.0250	13.602 134 636 613(21)
RR310	0.0018	13.602 134 636 612(20)
RR300	0.0037	13.602 134 636 614(21)

The measurement error in α^{-1} leads to a variation in the ionization energy equal to 9.3×10^{-12} eV, whereas a variation due to mass-input uncertainties, determined by a Monte Carlo simulation as in Section III A, amounts to 6.8×10^{-12} eV. Altogether,

$$\begin{aligned} E_I^{(D)} &= 13.602\,134\,636\,5430(283)_{\text{data}}(93)_{\alpha}(68)_{\text{mass}} \text{ eV} \\ &= 13.602\,134\,636\,543(31) \text{ eV} \end{aligned} \quad (45)$$

which agrees with the Standard Model prediction at the level of 2.3×10^{-12} .

V. SUMMARY AND DISCUSSION

This article presents a first attempt at fitting experimental atomic transition frequencies with the relativistic Ritz approach, a semi-empirical long-distance effective theory of hydrogen-like atoms. The quantum defect is written as a series expansion in low energy whose series coefficients parameterize physical effects whose range is shorter than the (infinite) range of the Coulomb interaction. Such effects include radiative QED corrections, as well as nuclear structure effects and any short-ranged beyond-the-standard-model dynamics.

Atomic hydrogen transition data was analyzed first in an exploratory way, considering various quantum defect truncations, or model choices. The best analysis yielded a value for the fine-structure constant, $\alpha =$

$1/137.035\,999\,185(25)$, in agreement with the determination using other methods and without using bound-state QED. Simultaneously, the ionization energy was found to

be $E_I^{(H)} = 13.598\,434\,599\,684(25)$ eV, in agreement with the Standard Model prediction at 1.8×10^{-12} . Some outlying transition data was discovered and, through continued cutting of outliers and re-analysis, I conclude that at least seven transitions are worth excluding from analysis. Predictions were made for these transitions which may be verified in future experiments.

As for atomic deuterium, there was insufficient data to simultaneously determine both the fine-structure constant and ionization energy. Using a fixed value of α coming from a recent electron g-factor measurement, the ionization energy was determined to be $E_I^{(D)} = 13.602\,134\,636\,543(31)$ eV, in agreement with the Standard Model at the level of 2.3×10^{-12} .

Historically, in order to measure α using spectroscopic data, bound-state QED has been employed to extract the Rydberg constant from which the determination of α is made. The nuclear radius also must be accounted for with that approach, but here such detailed modeling is not needed. The relativistic Ritz approach instead leverages the statistical power in using a modest number of atomic transitions, some of which have only been measured with modest precision. This may complement other approaches that apply bound-state QED to a smaller number of highly precise measurements. Another feature of the relativistic Ritz approach is that it can be used even if short-ranged beyond-the-standard-model phenomena are discovered to affect hydrogen-like atoms.

New and more precise measurements of atomic transitions, especially within hydrogen, deuterium, and positronium, may provide more accurate determinations of the fine-structure constant and ground state energies of simple atoms, thus allowing for a new way to test the Standard Model with precision atomic physics. Future work should determine what precision may be possible with future experimental data, but this is beyond the scope of the present article.

ACKNOWLEDGMENTS

I am grateful to Alexander Kramida for correspondence and for conversations with Gabe Duden, Maggie Rasmussen, Gloria Clausen, Frédéric Merkt, and Dylan Yost. This research was funded, in part, though a Charles A. Dana Research Fellowship at Norwich University.

-
- [1] Y. Fukuda *et al.* (Super-Kamiokande), Evidence for oscillation of atmospheric neutrinos, *Phys. Rev. Lett.* **81**, 1562 (1998), arXiv:hep-ex/9807003.
- [2] M. Dine and A. Kusenko, The Origin of the matter - antimatter asymmetry, *Rev. Mod. Phys.* **76**, 1 (2003), arXiv:hep-ph/0303065.
- [3] G. Bertone and D. Hooper, History of dark matter, *Rev. Mod. Phys.* **90**, 045002 (2018), arXiv:1605.04909 [astro-ph.CO].
- [4] M. S. Safronova, D. Budker, D. DeMille, D. F. J. Kimball, A. Derevianko, and C. W. Clark, Search for New Physics with Atoms and Molecules, *Rev. Mod. Phys.* **90**, 025008 (2018), arXiv:1710.01833 [physics.atom-ph].
- [5] D. B. Cassidy, Experimental progress in positronium laser physics, *Eur. Phys. J. D* **72**, 53 (2018).
- [6] P. Indelicato, QED tests with highly charged ions, *Journal of Physics B: Atomic, Molecular and Optical Physics* **52**, 232001 (2019).
- [7] K. Y. Khabarova and N. N. Kolachevsky, Proton charge radius, *Usp. Fiz. Nauk* **191**, 1095 (2021).
- [8] D. M. Jacobs, Relativistic Ritz approach to hydrogenic atoms, arXiv:2206.02494 (2022), arXiv:2206.02494 [physics.atom-ph].
- [9] D. M. Jacobs, Defect theory of positronium and non-trivial QED relations, *Phys. Rev. A* **104**, 032808 (2021), arXiv:2107.05505 [hep-ph].
- [10] E. Tiesinga, P. J. Mohr, D. B. Newell, and B. N. Taylor, CODATA recommended values of the fundamental physical constants: 2018*, *Rev. Mod. Phys.* **93**, 025010 (2021).
- [11] A. E. Kramida, A critical compilation of experimental data on spectral lines and energy levels of hydrogen, deuterium, and tritium, *Atom. Data Nucl. Data Tabl.* **96**, 586 (2010), [Erratum: *Atom. Data Nucl. Data Tabl.* **126**, 295–298 (2019)].
- [12] A. Kramida, Yu. Ralchenko, J. Reader, and and NIST ASD Team, NIST Atomic Spectra Database (ver. 5.9), [Online]. Available: <https://physics.nist.gov/asd> [2022, March 12]. National Institute of Standards and Technology, Gaithersburg, MD. (2021).
- [13] D. Hanneke, S. Fogwell, and G. Gabrielse, New Measurement of the Electron Magnetic Moment and the Fine Structure Constant, *Phys. Rev. Lett.* **100**, 120801 (2008), arXiv:0801.1134 [physics.atom-ph].
- [14] T. Aoyama, T. Kinoshita, and M. Nio, Theory of the Anomalous Magnetic Moment of the Electron, *Atoms* **7**, 28 (2019).
- [15] R. Bouchendira, P. Cladé, S. Guellati-Khélifa, F. m. c. Nez, and F. m. c. Biraben, New determination of the fine structure constant and test of the quantum electrodynamics, *Phys. Rev. Lett.* **106**, 080801 (2011).
- [16] R. H. Parker, C. Yu, W. Zhong, B. Estey, and H. Müller, Measurement of the fine-structure constant as a test of the Standard Model, *Science* **360**, 191 (2018), arXiv:1812.04130 [physics.atom-ph].
- [17] W. J. Huang, M. Wang, F. G. Kondev, G. Audi, and S. Naimi, The AME 2020 atomic mass evaluation (I). Evaluation of input data, and adjustment procedures, *Chin. Phys. C* **45**, 030002 (2021).
- [18] X. Fan, T. Myers, B. Sukra, and G. Gabrielse, Measurement of the electron magnetic moment, arXiv preprint arXiv:2209.13084 (2022).
- [19] L. Morel, Z. Yao, P. Cladé, and S. Guellati-Khélifa, Determination of the fine-structure constant with an accuracy of 81 parts per trillion, *Nature* **588**, 61 (2020).
- [20] W. Ritz, On a New Law of Series Spectra, *Astrophysical Journal* **28**, 237 (1908).
- [21] D. R. Hartree, The wave mechanics of an atom with a non-coulomb central field. part iii. term values and intensities in series in optical spectra, *Mathematical Proceedings of the Cambridge Philosophical Society* **24**, 426 (1928).
- [22] M. J. Seaton, Quantum defect theory, *Reports on Progress in Physics* **46**, 167 (1983).
- [23] D. M. Jacobs, Perturbative method for resolving contact interactions in quantum mechanics, *Phys. Rev. A* **100**, 062122 (2019), arXiv:1909.13407 [quant-ph].
- [24] D. M. Jacobs, Zenodo: Hydrogen and deuterium analysis (2022).
- [25] S. Sturm, F. Köhler, J. Zatorski, A. Wagner, Z. Harman, G. Werth, W. Quint, C. H. Keitel, and K. Blaum, High-precision measurement of the atomic mass of the electron, *Nature* **506**, 467 (2014).
- [26] F. Heiße, F. Köhler-Langes, S. Rau, J. Hou, S. Junck, A. Kracke, A. Mooser, W. Quint, S. Ulmer, G. Werth, K. Blaum, and S. Sturm, High-precision measurement of the proton's atomic mass, *Phys. Rev. Lett.* **119**, 033001 (2017).
- [27] S. Rau, F. Heiße, F. Köhler-Langes, S. Sasidharan, R. Haas, D. Renisch, C. E. Düllmann, W. Quint, S. Sturm, and K. Blaum, Penning trap mass measurements of the deuteron and the hd^+ molecular ion, *Nature* **585**, 43 (2020).
- [28] D. Anderson and K. Burnham, Model selection and multi-model inference, Second. NY: Springer-Verlag **63**, 10 (2004).
- [29] C. Bender and S. Orszag, *Advanced Mathematical Methods for Scientists and Engineers I: Asymptotic Methods and Perturbation Theory* (Springer, 1999).
- [30] A. D. Brandt, S. F. Cooper, C. Rasor, Z. Burkley, D. C. Yost, and A. Matveev, Measurement of the $2S_{1/2}$ - $8D_{5/2}$ Transition in Hydrogen, *Phys. Rev. Lett.* **128**, 023001 (2022), arXiv:2111.08554 [physics.atom-ph].
- [31] A. Grinin, A. Matveev, D. C. Yost, L. Maisenbacher, V. Wirthl, R. Pohl, T. W. Hänsch, and T. Udem, Two-photon frequency comb spectroscopy of atomic hydrogen, *Science* **370**, 1061 (2020).
- [32] W. Ubachs, Crisis and catharsis in atomic physics, *Science* **370**, 1033 (2020).
- [33] V. A. Yerokhin, K. Pachucki, and V. Patkóš, Theory of the lamb shift in hydrogen and light hydrogen-like ions, *Annalen der Physik* **531**, 1800324 (2019).
- [34] P. Zhao, W. Lichten, H. Layer, and J. Bergquist, Remeasurement of the rydberg constant, *Physical Review A* **34**, 5138 (1986).

TABLE VII. Hydrogen transitions. References are given for those taken from sources other than the compilation in Ref. [12].

Number	Transition	Frequency (GHz)
1	$1S_{1/2} \rightarrow 12P_{3/2}$	3 265 251(71)
2	$1S_{1/2} \rightarrow 12P_{1/2}$	3 265 251(71)
3	$1S_{1/2} \rightarrow 11P_{3/2}$	3 260 921(71)
4	$1S_{1/2} \rightarrow 11P_{1/2}$	3 260 921(71)
5	$1S_{1/2} \rightarrow 10P_{3/2}$	3 255 182(71)
6	$1S_{1/2} \rightarrow 10P_{1/2}$	3 255 182(71)
7	$1S_{1/2} \rightarrow 9P_{3/2}$	3 247 491(70)
8	$1S_{1/2} \rightarrow 9P_{1/2}$	3 247 491(70)
9	$1S_{1/2} \rightarrow 8P_{3/2}$	3 236 699(70)
10	$1S_{1/2} \rightarrow 8P_{1/2}$	3 236 699(70)
11	$1S_{1/2} \rightarrow 7P_{3/2}$	3 220 981(69)
12	$1S_{1/2} \rightarrow 7P_{1/2}$	3 220 981(69)
13	$1S_{1/2} \rightarrow 6P_{3/2}$	3 196 760(72)
14	$1S_{1/2} \rightarrow 6P_{1/2}$	3 196 760(72)
15	$1S_{1/2} \rightarrow 5P_{3/2}$	3 156 567(13)
16	$1S_{1/2} \rightarrow 5P_{1/2}$	3 156 567(13)
17	$1S_{1/2} \rightarrow 4P_{3/2}$	3 082 569(60)
18	$1S_{1/2} \rightarrow 4P_{1/2}$	3 082 569(60)
19	$1S_{1/2} \rightarrow 3S_{1/2}$	2 922 743.278 665 79(72) [31]
20	$1S_{1/2} \rightarrow 3P_{3/2}$	2 922 728.6(8.5)
21	$1S_{1/2} \rightarrow 3P_{1/2}$	2 922 728.6(8.5)
22	$1S_{1/2} \rightarrow 2P_{3/2}$	2 466 068.0(4.1)
23	$1S_{1/2} \rightarrow 2P_{1/2}$	2 466 068.0(4.1)
24	$1S_{1/2} \rightarrow 2S_{1/2}$	2 466 061.413 187 070(30)
25	$2S_{1/2} \rightarrow 12D_{5/2}$	799 191.727 4038(64)
26	$2S_{1/2} \rightarrow 12D_{3/2}$	799 191.710 473(11)
27	$2S_{1/2} \rightarrow 10D_{5/2}$	789 144.886 412(39)
28	$2S_{1/2} \rightarrow 8D_{5/2}$	770 649.561 5709(20) [30]
29	$2S_{1/2} \rightarrow 8D_{3/2}$	770 649.504 4499(79)
30	$2S_{1/2} \rightarrow 8S_{1/2}$	770 649.350 0121(99)

TABLE VIII. Continuation of Table VII.

Number	Transition	Frequency (GHz)
31	$2S_{1/2} \rightarrow 4D_{5/2}$	616 521.843 441(24)
32	$2S_{1/2} \rightarrow 4P_{3/2}$	616 521.388 672(10)
33	$2S_{1/2} \rightarrow 4S_{1/2}$	616 520.150 637(10)
34	$2S_{1/2} \rightarrow 4P_{1/2}$	616 520.017 568(15)
35	$2P_{1/2} \rightarrow 3D_{3/2}$	456 685.8528(17)
36	$2S_{1/2} \rightarrow 3P_{3/2}$	456 684.800 11(28)
37	$2S_{1/2} \rightarrow 3P_{1/2}$	456 681.549 89(28)
38	$2P_{3/2} \rightarrow 3D_{5/2}$	456 675.9681(42)
39	$2P_{1/2} \rightarrow 2P_{3/2}$	10.969 13(10)
40	$2S_{1/2} \rightarrow 2P_{3/2}$	9.911 202(13)
41	$3S_{1/2} \rightarrow 3D_{5/2}$	4.013 162(48)
42	$3P_{1/2} \rightarrow 3P_{3/2}$	3.250 31(39)
43	$3P_{1/2} \rightarrow 3D_{3/2}$	3.2449(32)
44	$3S_{1/2} \rightarrow 3P_{3/2}$	2.9334(11)
45	$3S_{1/2} \rightarrow 3D_{3/2}$	2.929 95(86)
46	$4S_{1/2} \rightarrow 4D_{5/2}$	1.692 98(38)
47	$4P_{1/2} \rightarrow 4D_{3/2}$	1.3711(12)
48	$4P_{1/2} \rightarrow 4P_{3/2}$	1.370 86(25)
49	$4S_{1/2} \rightarrow 4P_{3/2}$	1.237 79(31)
50	$4S_{1/2} \rightarrow 4D_{3/2}$	1.2352(20)
51	$3D_{3/2} \rightarrow 3D_{5/2}$	1.0831(31)
52	$3P_{3/2} \rightarrow 3D_{5/2}$	1.0780(12)
53	$2P_{1/2} \rightarrow 2S_{1/2}$	1.057 8470(9.0)
54	$5P_{1/2} \rightarrow 5D_{3/2}$	0.7037(66)
55	$5S_{1/2} \rightarrow 5P_{3/2}$	0.622(12)
56	$4P_{3/2} \rightarrow 4D_{5/2}$	0.4557(16)
57	$3P_{1/2} \rightarrow 3S_{1/2}$	0.314 819(50)
58	$5P_{3/2} \rightarrow 5D_{5/2}$	0.2320(31)
59	$4P_{1/2} \rightarrow 4S_{1/2}$	0.133 18(59)
60	$3D_{3/2} \rightarrow 3P_{3/2}$	0.005 45(89)

TABLE XXIII. Deuterium transitions from Ref. [12].

Number	Transition	Frequency (GHz)
1	$1S_{1/2} \rightarrow 2P_{3/2}$	2 466 742.2(1.0)
2	$1S_{1/2} \rightarrow 2S_{1/2}$	2 466 732.407 521 70(14)
3	$2S_{1/2} \rightarrow 12D_{5/2}$	799 409.184 9668(64)
4	$2S_{1/2} \rightarrow 12D_{3/2}$	799 409.168 0372(85)
5	$2S_{1/2} \rightarrow 10D_{5/2}$	789 359.610 240(39)
6	$2P_{1/2} \rightarrow 9D_{3/2}$	781 645.75(31)
7	$2P_{3/2} \rightarrow 9D_{5/2}$	781 634.79(31)
8	$2P_{1/2} \rightarrow 8D_{3/2}$	770 860.36(22)
9	$2S_{1/2} \rightarrow 8D_{5/2}$	770 859.252 8501(59)
10	$2S_{1/2} \rightarrow 8D_{3/2}$	770 859.195 7016(59)
11	$2S_{1/2} \rightarrow 8S_{1/2}$	770 859.041 2472(79)
12	$2P_{3/2} \rightarrow 8D_{5/2}$	770 849.56(22)
13	$2P_{1/2} \rightarrow 7D_{3/2}$	755 128.601(57)
14	$2P_{3/2} \rightarrow 7D_{5/2}$	755 117.702(57)
15	$2P_{1/2} \rightarrow 6D_{3/2}$	730 890.310(53)
16	$2P_{3/2} \rightarrow 6D_{5/2}$	730 879.477(71)
17	$2P_{1/2} \rightarrow 5D_{3/2}$	690 691.823(48)
18	$2P_{3/2} \rightarrow 5D_{5/2}$	690 681.098(64)
19	$2P_{1/2} \rightarrow 4D_{3/2}$	616 690.175(38)
20	$2S_{1/2} \rightarrow 4D_{5/2}$	616 689.59 6718(37)
21	$2S_{1/2} \rightarrow 4P_{3/2}$	616 689.141 73(16)
22	$2S_{1/2} \rightarrow 4S_{1/2}$	616 687.903 573(20)
23	$2S_{1/2} \rightarrow 4P_{1/2}$	616 687.769 99(19)
24	$2P_{3/2} \rightarrow 4D_{5/2}$	616 679.760(51)
25	$2P_{1/2} \rightarrow 3D_{3/2}$	456 810.1143(21)
26	$2S_{1/2} \rightarrow 3P_{3/2}$	456 809.062 66(28)
27	$2S_{1/2} \rightarrow 3P_{1/2}$	456 805.811 72(28)
28	$2P_{3/2} \rightarrow 3D_{5/2}$	456 800.2259(16)
29	$2P_{3/2} \rightarrow 3S_{1/2}$	456 796.254(28)
30	$2S_{1/2} \rightarrow 2P_{3/2}$	9.912 59(29)
31	$3P_{1/2} \rightarrow 3P_{3/2}$	3.2508(11)
32	$3S_{1/2} \rightarrow 3P_{3/2}$	2.9351(49)
33	$4P_{1/2} \rightarrow 4P_{3/2}$	1.371 80(31)
34	$2P_{1/2} \rightarrow 2S_{1/2}$	1.059 281(60)
35	$3P_{1/2} \rightarrow 3S_{1/2}$	0.315 31(40)
36	$4P_{1/2} \rightarrow 4S_{1/2}$	0.1332(59)